The Astrophysical Journal, 949:64 (6pp), 2023 June 1 https://doi.org/10.3847/1538-4357/acc949

Implications for Primordial Black Holes from Cosmological Constraints on Scalar-induced Gravitational Waves

Junsong Cang[1,2,3], Yin-Zhe Ma[4,5,6,7], and Yu Gao[1]
[1] Key Laboratory of Particle Astrophysics, Institute of High Energy Physics, Chinese Academy of Sciences, Beijing, 100049, People's Republic of China; ma@ukzn.ac.za
[2] School of Physical Sciences, University of Chinese Academy of Sciences, Beijing, 100049, People's Republic of China; gaoyu@ihep.ac.cn
[3] Scuola Normale Superiore, Piazza dei Cavalieri 7, I-56126 Pisa, Italy
[4] School of Chemistry and Physics, University of KwaZulu-Natal, Westville Campus, Private Bag X54001, Durban, 4000, South Africa
[5] NAOCUKZN Computational Astrophysics Centre (NUCAC), University of KwaZulu-Natal, Durban, 4000, South Africa
[6] National Institute for Theoretical and Computational Sciences (NITheCS), South Africa
[7] Department of Physics, Stellenbosch University, Matieland 7602, South Africa
Received 2023 January 13; revised 2023 March 20; accepted 2023 March 28; published 2023 May 31

Abstract

Sufficiently large scalar perturbations in the early universe can create overdense regions that collapse into primordial black holes (PBHs). This process is accompanied by the emission of scalar-induced gravitational waves that behave like an extra radiation component, thus contributing to the relativistic degrees of freedom ($N_{\rm eff}$). We show that the cosmological constraints on $N_{\rm eff}$ can be used to pose stringent limits on PBHs created from this particular scenario as well as the relevant small-scale curvature perturbation ($\mathcal{P}_{\mathcal{R}}(k)$). We show that the combination of cosmic microwave background (CMB), baryon acoustic oscillation, and Big Bang nucleosynthesis data sets can exclude supermassive PBHs with peak mass $M_{\bullet} \in [5 \times 10^5, 5 \times 10^{10}]\, M_{\odot}$ as the major component of dark matter, while the detailed constraints depend on the shape of the PBHs' mass distribution. A future CMB mission such as CMB-S4 can greatly broaden this constraint window to $M_{\bullet} \in [8 \times 10^{-5}, 5 \times 10^{10}]\, M_{\odot}$, covering substellar masses. These limits on PBHs correspond to a tightened constraint on $\mathcal{P}_{\mathcal{R}}$ on scales of $k \in [10, 10^{22}]\,{\rm Mpc}^{-1}$, much smaller than those probed by direct CMB and large-scale structure power spectra.

Unified Astronomy Thesaurus concepts: Cosmological perturbation theory (341)

1. Introduction

Large density fluctuations in the early universe can lead to gravitational collapse of overdense regions and form primordial black holes (PBHs; Hawking 1971; Carr & Hawking 1974; Carr 1975). PBHs have been proposed to explain a range of observed black hole conundrums (Carr et al. 2021a), such as the existence of supermassive black holes (Bean & Magueijo 2002) and black hole merging events seen by LIGO and Virgo (Abbott et al. 2019; Hütsi et al. 2021; Jedamzik 2021). PBHs are also considered as a dark matter (DM) candidate (Carr et al. 2016; Carr & Kuhnel 2020, 2022) and their abundance has been constrained via various cosmological and astrophysical observations (Khlopov 2010; Tashiro & Sugiyama 2013; Belotsky et al. 2014, 2019; Carr et al. 2016, 2021b; Carr & Kuhnel 2020, 2022; Ali-Haïmoud & Kamionkowski 2017; Clark et al. 2017, 2018; Wang et al. 2018, 2023; Laha 2019; Chen et al. 2020; Laha et al. 2020; Ashoorioon et al. 2021a, 2021b, 2022; Domènech et al. 2021a, 2021b; Hütsi et al. 2021; Vaskonen & Veermäe 2021; Ray et al. 2021; Yang 2021; Cang et al. 2022; Auffinger 2022; Karam et al. 2023; Mittal et al. 2022; Zhou et al. 2022; see Carr & Kuhnel 2020 for a review).

There are a plethora of mechanisms through which PBHs can be produced (Carr et al. 2021b), such as bubble collisions (Crawford & Schramm 1982; Hawking et al. 1982; La & Steinhardt 1989) and the collapse of cosmic strings (Hogan 1984; Hawking 1989; Polnarev & Zembowicz 1991; Hansen et al. 2000). Here we focus on one particular scenario in which PBHs are formed from overdensities produced by an inflation-induced enhancement of primordial curvature perturbation (Carr et al. 2010; Inomata & Nakama 2019; Chen et al. 2021; Kimura et al. 2021; Wang et al. 2023). At large scales $k \lesssim 1\,{\rm Mpc}^{-1}$, the curvature perturbation power spectrum $\mathcal{P}_{\mathcal{R}}$ has been precisely measured by cosmic microwave background (CMB) and large-scale structure (LSS) observations (Hunt & Sarkar 2015; Planck Collaboration et al. 2020), but the small-scale power is still poorly constrained (Byrnes et al. 2019; Inomata & Nakama 2019; Pi & Sasaki 2020; Chen et al. 2021; Kimura et al. 2021; Yuan & Huang 2021; Wang et al. 2023). Thus, the enhanced small-scale $\mathcal{P}_{\mathcal{R}}$ can potentially produce enough PBHs to explain *all* dark matter without violating the existing observational bounds.

Associated with PBH production, enhanced $\mathcal{P}_{\mathcal{R}}$ inevitably generates a scalar-induced gravitational wave (SIGW) at second order (Carbone & Matarrese 2005; Nakamura 2007; Chen et al. 2021; Vaskonen & Veermäe 2021; Yuan & Huang 2021; Karam et al. 2023), which can potentially be observed by gravitational wave (GW) detectors like Taiji (Hu & Wu 2017) and LISA (Amaro-Seoane et al. 2017). After horizon-crossing, an SIGW can be considered as dark radiation (DR; Chacko et al. 2015; Serpico 2019; Takahashi & Yamada 2019) in that it freestreams with an energy density redshifting as $(1+z)^4$ (Inomata & Nakama 2019; Chen et al. 2021). From a cosmological point of view, the gravitational behavior of an SIGW is indistinguishable from that of a relativistic species such as the massless neutrino. Therefore, just like other forms of dark radiation (e.g., primordial gravitational waves (Meerburg et al. 2015; Aich et al. 2020),

axions (Green et al. 2019), and sterile neutrinos (Takahashi & Yamada 2019; Green et al. 2019)), the energy density of SIGW DR can be parameterized by an additional effective degree of freedom

$$\Delta N_{\rm eff} \equiv N_{\rm eff} - N_{\rm eff}^{\rm SM}, \tag{1}$$

where $N_{\rm eff}$ describes the total effects of relativistic species containing both neutrinos and SIGWs, and $N_{\rm eff}^{\rm SM} = 3.046$ is the prediction from the standard model (SM) of particle physics (Mangano et al. 2002, 2005; de Salas & Pastor 2016).

As a measure of cosmic radiation density, a higher $N_{\rm eff}$ can delay radiation–matter equality and change the size of the sound horizon (Aich et al. 2020), which can leave distinctive features on CMB anisotropies (Hou et al. 2013; Follin et al. 2015), baryon acoustic oscillations (BAOs), and Big Bang nucleosynthesis (BBN, Wallisch 2018). Currently the leading $\Delta N_{\rm eff}$ constraint is set by measuring the damping tail and the phase shift in the CMB anisotropy spectrum (Hou et al. 2013; Follin et al. 2015; Ade et al. 2016; Wallisch 2018; Aich et al. 2020), which reads $\Delta N_{\rm eff} < 0.3$ at 95% confidence level (C.L.) from the latest Planck CMB data (Planck Collaboration et al. 2020). Future CMB missions are expected to provide significant improvements on $\Delta N_{\rm eff}$ (Abazajian et al. 2016; Di Valentino et al. 2018; Hanany et al. 2019). For example, the CMB Stage IV (S4) experiment is aiming to constrain $\Delta N_{\rm eff} < 0.027$ at 2σ C.L. (Abazajian et al. 2016; Baumann et al. 2016a, 2016b; Wallisch 2018).

Here we use the SIGW upper bounds inferred from cosmological constraints on $\Delta N_{\rm eff}$ to place limits on both small-scale $\mathcal{P}_\mathcal{R}$ and the associated PBH abundance. The structure of this paper is as follows: Section 2 reviews PBH production induced by enhanced curvature perturbation. Section 3 discusses the energy density of SIGWs and its connection with $N_{\rm eff}$. Our results are presented in Section 4 and we conclude in Section 5.

2. PBH Model

In order for inflation to produce density fluctuation required for efficient PBH formation, the primordial curvature perturbation power spectrum $\mathcal{P}_\mathcal{R}$ needs to be boosted to 10^{-2} on small scales ($k \gtrsim 1\ {\rm Mpc}^{-1}$) (Josan et al. 2009; Bringmann et al. 2012; Garcia-Bellido & Ruiz Morales 2017; Pi & Sasaki 2020; Chen et al. 2021; Green & Kavanagh 2021; Karam et al. 2023), which can be realised in several inflation theories (Kawasaki et al. 1998; Yokoyama 1998a; Kohri et al. 2013; Garcia-Bellido & Ruiz Morales 2017; Cai et al. 2020; Kannike et al. 2017; Pi & Sasaki 2020). As a good approximation for a wide range of curvature perturbations (Inomata & Nakama 2019; Pi & Sasaki 2020; Chen et al. 2021; Domènech 2021; Yuan & Huang 2021), we adopt a log-normal $\mathcal{P}_\mathcal{R}$ model peaked at the scale $k_\bullet$, which was motivated in the Horndeski theory of gravity (Inomata & Nakama 2019; Chen et al. 2021):

$$\mathcal{P}_\mathcal{R} = A_{\rm s}\left(\frac{k}{k_*}\right)^{n_{\rm s}-1}\left[1 + \frac{A}{\sqrt{2\pi\sigma^2}}{\rm e}^{-\left(\ln\frac{k}{k_\bullet}\right)^2\Big/2\sigma^2}\right], \tag{2}$$

where $A_{\rm s} = 2.1\times10^{-9}$ and $n_{\rm s} = 0.9665$ are the amplitude and spectral index of primordial fluctuations fixed at the pivot scale $k_* = 0.05\ {\rm Mpc}^{-1}$ (Planck Collaboration et al. 2020). Model parameters A, $k_\bullet$, and σ describe the amplitude, location, and width of the enhanced peak. For large scales ($k \ll k_\bullet$) or for $A \to 0$, $\mathcal{P}_\mathcal{R}$ is reduced to a power-law primordial spectrum.

Once the large scalar fluctuations have crossed the Hubble radius during radiation-dominated era, the overdensity above a certain threshold ($\delta_{\rm c} \simeq 0.45$, see, e.g., Harada et al. 2013; Musco & Miller 2013; Carr & Kuhnel 2020[8]) can gravitationally collapse into a PBH with mass (Carr et al. 2010; Nakama et al. 2017; Özsoy et al. 2018; Chen et al. 2021),

$$M = 3.16\times10^{12}\left(\frac{\gamma}{0.2}\right)\left(\frac{g_*(T)}{106.75}\right)^{-1/6}\left(\frac{k}{{\rm Mpc}^{-1}}\right)^{-2} M_\odot, \tag{3}$$

where γ is the collapse efficiency, for which we adopt a typical value of $\gamma = 0.2$ (Carr 1975; Carr et al. 2010; Özsoy et al. 2018; Chen et al. 2021). $g_*(T)$ is the total number of effectively massless degrees of freedom (those species with $m \ll T$) at horizon-crossing ($k = aH$), where we adopted SM particle content $({\rm SU(3)_C}\otimes{\rm SU(2)_L}\otimes{\rm U(1)_Y}$ theory, Kolb & Turner 1990; Wallisch 2018).

We use model of Press & Schechter (1974) to calculate the fraction of the universe's density collapsing into PBHs with mass M (Carr 1975; Özsoy et al. 2018; Carr & Kuhnel 2020; Chen et al. 2021):

$$\begin{aligned}\beta(M) &\equiv \rho_\bullet/\rho_{\rm cr}(z)\\ &= 2\int_{\delta_{\rm c}}^{\infty} d\delta \frac{1}{\sqrt{2\pi\bar\sigma^2}}\exp\left(-\frac{\delta^2}{2\bar\sigma^2}\right)\\ &\simeq \sqrt{\frac{2\bar\sigma^2}{\pi\delta_{\rm c}^2}}\exp\left(-\frac{\delta_{\rm c}^2}{2\bar\sigma^2}\right),\end{aligned} \tag{4}$$

where $\rho_\bullet$ and $\rho_{\rm cr}(z)$ are the PBH density and the critical density of the universe at the collapsing time. In deriving the third equality in Equation (4) we used $\delta_{\rm c} > \bar\sigma$, which remains valid for all scenarios we explored. $\bar\sigma^2$ is the variance of density fluctuations at the scale k^{-1} (Young et al. 2014; Özsoy et al. 2018; Chen et al. 2021):

$$\bar\sigma^2(M) = \frac{16}{81}\int d\ln k' \left(\frac{k'}{k}\right)^4 \mathcal{P}_\mathcal{R}(k') W^2\left(\frac{k'}{k}\right), \tag{5}$$

where the function $k(M)$ is defined via Equation (3). $W(x)$ is a window function, for which we use $\exp(-x^2/2)$ (Özsoy et al. 2018; Chen et al. 2021).

Since PBHs behave like matter, $\rho_\bullet/\rho_{\rm cr}$ grows inversely proportionally to temperature until matter–radiation equality, and the current distribution of PBH abundance in different masses can be estimated via (see also Young et al. 2014; Inomata et al. 2017; Özsoy et al. 2018; Chen et al. 2021)

$$\begin{aligned}\Phi &\equiv \frac{d f_{\rm bh}}{d\ln M}\\ &= 0.28\left(\frac{\beta}{10^{-8}}\right)\left(\frac{\gamma}{0.2}\right)^{3/2}\left(\frac{g_*}{106.75}\right)^{-1/4}\left(\frac{M}{M_\odot}\right)^{-1/2},\end{aligned} \tag{6}$$

where $f_{\rm bh} \equiv \rho_\bullet/\rho_{\rm c}$ is the fraction of cold dark matter in the form of PBHs. For convenience, we describe the distribution calculated from Equation (6) with a log-normal

[8] A simple analytic estimate would give $\delta_{\rm c} \sim 0.3$ (Carr 1975), but our value was suggested from recent analytic and numerical analyses (Harada et al. 2013; Musco & Miller 2013; Carr & Kuhnel 2020).

parameterization (Dolgov & Silk 1993; Green 2016; Carr et al. 2017; Carr & Kuhnel 2020; Cang et al. 2022):

$$\Phi = f_{\rm bh}\frac{1}{\sqrt{2\pi}\,\sigma_\bullet}\exp\left[-\frac{\ln(M/M_\bullet)^2}{2\sigma_\bullet^2}\right], \tag{7}$$

which provides an excellent fit to the actual profile. Model parameters $M_\bullet$ and $\sigma_\bullet$ describe peak PBH mass and distribution width respectively, and their values are calculated using a least-squares fitting method.

3. SIGWs as Dark Radiation

In addition to forming PBHs, scalar perturbations also change the radiation quadruple moment and generate GWs at second order, which carry an energy density $\rho_{\rm GW}$ that redshifts as radiation after the horizon-crossing (Inomata & Nakama 2019; Chen et al. 2021), $\rho_{\rm GW}\propto(1+z)^4$. At the present day, the GW energy density parameter $\Omega_{\rm GW}\equiv(\rho_{\rm GW}/\rho_{\rm cr})_{z=0}$ follows the distribution (Ando et al. 2018; Kohri & Terada 2018; Inomata & Nakama 2019)

$$\begin{aligned}\Psi &\equiv \frac{d\Omega_{\rm GW}}{d\,\ln k}\\ &= 0.29\,\Omega_{\rm r}\left(\frac{106.75}{g_*}\right)^{1/3}\\ &\quad\times\int_0^\infty dv\int_{|1-v|}^{1+v}du\left[\frac{4v^2-(1-u^2+v^2)^2}{4u^2v^2}\right]^2\\ &\quad\times\left(\frac{u^2+v^2-3}{2uv}\right)^4 F(u,v)\mathcal{P}_\mathcal{R}(kv)\mathcal{P}_\mathcal{R}(ku),\end{aligned} \tag{8}$$

$$\begin{aligned}F(u,v) = &\left(\ln\left|\frac{3-(u+v)^2}{3-(u-v)^2}\right| - \frac{4uv}{u^2+v^2-3}\right)^2\\ &+\pi^2\Theta(u+v-\sqrt{3}),\end{aligned} \tag{9}$$

where $\Omega_{\rm r}=9.1\times10^{-5}$ is the present fractional radiation density assuming massless neutrinos.

After neutrino decoupling, the cosmic radiation energy density ($\rho_{\rm r}$) is a sum of CMB photon (γ), neutrino (ν), and GW densities:

$$\rho_{\rm r} = \rho_\gamma + \rho_\nu + \rho_{\rm GW}, \tag{10}$$

where

$$\begin{aligned}\rho_\gamma &= \frac{\pi^2}{15}T_\gamma^4,\\ \rho_\nu + \rho_{\rm GW} &= \frac{7\pi^2}{120}N_{\rm eff}\,T_\nu^4.\end{aligned} \tag{11}$$

Here $T_\gamma = 2.728(1+z)$ K and $T_\nu=(4/11)^{1/3}T_\gamma$ are the temperatures of CMB and neutrinos respectively. Because the behavior of GW density mimics that of neutrinos, Equation (11) counts the contribution of GWs to the effective number of neutrino species as $\Delta N_{\rm eff}$ (Equation (1)). Comparing $\rho_{\rm GW}=\Omega_{\rm GW}\rho_{\rm cr}(1+z)^4$ with Equation (11), one can see that

$$\Delta N_{\rm eff} = 8.3\times10^4\,\Omega_{\rm GW}(\boldsymbol{\theta}), \tag{12}$$

where $\boldsymbol{\theta}$ indicates the model parameters. Depending on the choice of parameterization, $\boldsymbol{\theta}$ can be either the $\mathcal{P}_\mathcal{R}$ parameters (A, σ, $k_\bullet$) defined in Equation (2) or the PBH parameters ($f_{\rm bh}$, $\sigma_\bullet$, $M_\bullet$) defined in Equation (7). For a given set of $\mathcal{P}_\mathcal{R}$ parameters, the value of $\Omega_{\rm GW}$ is directly determined by integrating Equation (8). To obtain the relation between $\Omega_{\rm GW}$ and PBH parameters, we constructed a three-dimensional grid in $\mathcal{P}_\mathcal{R}$ parameter space and calculated $\Omega_{\rm GW}$ and ($f_{\rm bh}$, $\sigma_\bullet$, $M_\bullet$) for each point on the grid. Using the large discrete sample of the function $\Omega_{\rm GW}(f_{\rm bh},\sigma_\bullet,M_\bullet)$ obtained in the process, we then built an interpolation function to calculate $\Omega_{\rm GW}$ for any ($f_{\rm bh}$, $\sigma_\bullet$, $M_\bullet$) parameter values in between.

To derive our PBH and $\mathcal{P}_\mathcal{R}$ constraints, we use the $N_{\rm eff}$ limits from Planck Collaboration et al. (2020), which give $N_{\rm eff}=3.04\pm0.22$ at 95% C.L. for Planck+BAO+BBN data (hereafter PBB).[9] Using Gaussian statistics, this can be inverted to a 95% C.L. upper bound of $\Delta N_{\rm eff}<0.175$. We also study the prospective constraints from a future CMB Stage IV experiment, which is expected to constrain $\Delta N_{\rm eff}<0.027$ at 95% confidence level (Abazajian et al. 2016; Baumann et al. 2016a, 2016b; Wallisch 2018). Combining the current and future constraints, we have

$$\Delta N_{\rm eff} < \begin{cases}0.175 & \text{Planck + BAO + BBN (PBB)}\\ 0.027 & \text{CMB Stage IV (S4).}\end{cases} \tag{13}$$

Through Equation (12), Equation (13) is inverted to the upper bounds on SIGW density at 95% C.L.:

$$\Omega_{\rm GW} < \begin{cases}2.11\times10^{-6} & \text{(PBB)}\\ 3.25\times10^{-7} & \text{(S4).}\end{cases} \tag{14}$$

In the following, we will substitute Equation (2) into Equation (8) to calculate $\Omega_{\rm GW}$ or calculate it numerically using the $\Omega_{\rm GW}(f_{\rm bh},\sigma_\bullet,M_\bullet)$ interpolation function, and then we will use the upper bound in Equation (14) to constrain the model parameters. We also notice that because of the positive correlation between $N_{\rm eff}$ and H_0, adopting a different value of H_0 may lead to a shift of the posterior distribution of $N_{\rm eff}$. In recent years, measurements from the local distance ladder (Riess et al. 2016, 2018, 2022) have given a higher value of H_0 than the CMB (Aiola et al. 2020; Planck Collaboration et al. 2020; Balkenhol et al. 2022) and BAO measurements (Schöneberg et al. 2022), which are inconsistent with each other at almost 5σ C.L. (Verde et al. 2019). However, we notice that there is still a lot of debate on the potential systematics of Cepheid measurements (Efstathiou 2020, 2021; Freedman et al. 2020), which requires more data in the future to clarify these measurements. The uncertainty of $N_{\rm eff}$ associated with this ongoing debates on anchor galaxy distance certainly exceeds the scope of this paper, but we alert the reader to the potential effect of this on $N_{\rm eff}$ measurement.

4. Results

For given σ and k, $\mathcal{P}_\mathcal{R}$ is determined by the parameters $k_\bullet$ and A. Once we set $k_\bullet = k\exp[(1-n_{\rm s})\sigma^2]$, which gives a $\mathcal{P}_\mathcal{R}$ spectrum that peaks at k (see Equation (2)), the upper bound on $\mathcal{P}_\mathcal{R}(k)$ can be obtained by fixing A to its upper limit given by

[9] Note that there are several updated $N_{\rm eff}$ constraints from more recent CMB data sets, e.g., Planck and ACTPol jointly constrain $N_{\rm eff}=2.74\pm0.17$ at 68% C.L. (Aiola et al. 2020), which is lower than the standard model $N_{\rm eff}=3.046$ by 1.8σ C.L. This might be due to unaccounted for systematics in the data. The SPT-3G and Planck data give $N_{\rm eff}=3.00\pm0.18$ at 68% C.L (Balkenhol et al. 2022), which has a larger error than the PBB limits.

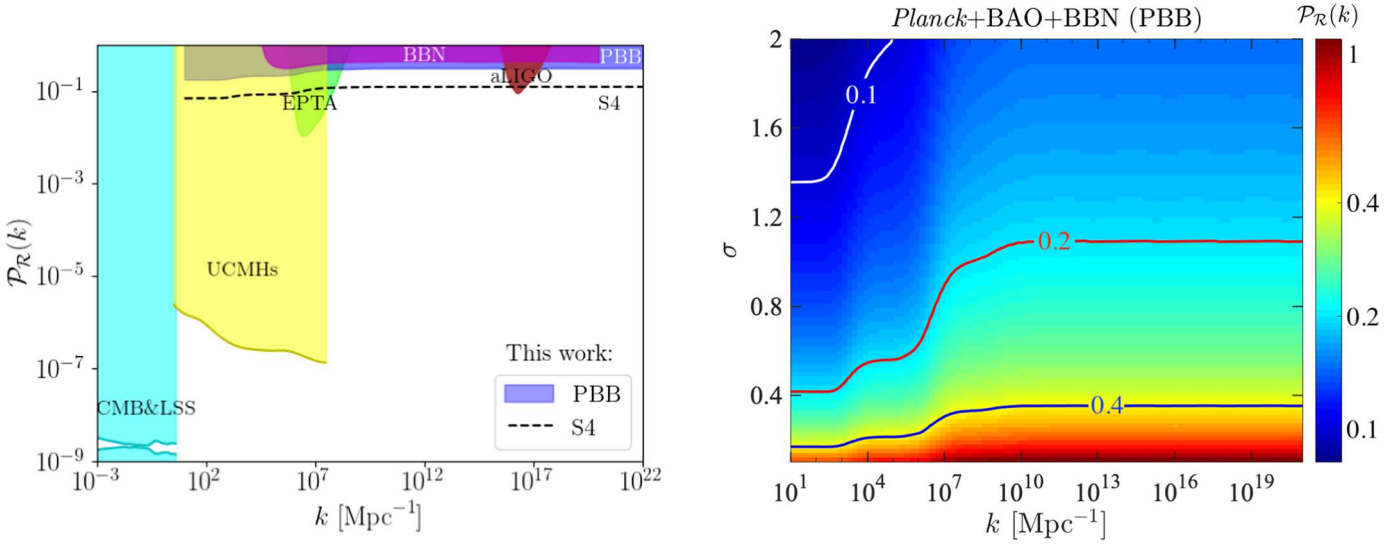

Figure 1. Left: comparison of $\mathcal{P}_\mathcal{R}$ constraints. The shaded regions show the excluded parameter space. We indicate limits derived in this work for $\sigma = 0.5$ by the blue shaded region and black dashed line, corresponding to the space currently excluded from PBB and the forecasted S4 upper bounds respectively. Regions in cyan and yellow indicate the constraints from CMB and LSS (Hunt & Sarkar 2015), and the nondetection of γ-rays from ultracompact minihalos (UCMHs, Bringmann et al. 2012). Regions in magenta, green, and brown show the exclusion of $\mathcal{P}_\mathcal{R}$ with width of $\sigma = 0.5$, from Big Bang nucleosynthesis (BBN, Kohri & Terada 2018; Inomata & Nakama 2019), the European Pulsar Timing Array (EPTA), and Advanced LIGO (aLIGO, Inomata & Nakama 2019). Right: our $\mathcal{P}_\mathcal{R}$ upper bounds for different k and σ parameters, set by the current PBB data sets. Prospective $\Delta N_{\rm eff}$ limits from S4 can uniformly improve current PBB constraints by 60%.

Equation (14). To avoid overlapping with existing constraints at large scales (Hunt & Sarkar 2015), we restrict the solution to the range $k > 10\,\mathrm{Mpc}^{-1}$, which corresponds to $M_\bullet < 5 \times 10^{10}\,M_\odot$ from Equation (3).

As shown in Figure 1, in the majority of parameter space we explored, our results show that PBB constrains $\mathcal{P}_\mathcal{R}$ to be $\sim\mathcal{O}(10^{-1})$. The constraint becomes more stringent for a wider spectral width σ, which is because the peak amplitude of $\mathcal{P}_\mathcal{R}$ is roughly inversely proportional to σ. For a sharp spectrum with $\sigma = 0.1$, our constraint yields $\mathcal{P}_\mathcal{R} \lesssim 1$, whereas the limit tightens to $\mathcal{P}_\mathcal{R} \lesssim 0.1$ for $\sigma = 2$. In most cases, the linear part in Equation (2) can be safely ignored, so that $\mathcal{P}_\mathcal{R} \propto A$ and $\Omega_{\rm GW} \propto A^2$, therefore our $\mathcal{P}_\mathcal{R}$ upper limit is proportional to the maximally allowed $\sqrt{\Omega_{\rm GW}}$. Therefore, compared to PBB, the CMB-S4 experiment will uniformly improve its $\mathcal{P}_\mathcal{R}$ constraint by 60% on all scales.

The left panel of Figure 1 compares our PBB and S4 results with other leading $\mathcal{P}_\mathcal{R}$ constraints from different astrophysical data (Bringmann et al. 2012; Hunt & Sarkar 2015; Inomata & Nakama 2019). At $k < 4\,\mathrm{Mpc}^{-1}$, $\mathcal{P}_\mathcal{R}$ is well measured by CMB anisotropy and LSS to $\sim 2 \times 10^{-9}$ (Hunt & Sarkar 2015). For $k = [4,\ 3 \times 10^7]\,\mathrm{Mpc}^{-1}$, the nondetection of gamma rays from ultracompact minihalos (UCMHs) gives $\mathcal{P}_\mathcal{R} \lesssim 10^{-6}$ (Bringmann et al. 2012). All other limits shown in Figure 1 are for $\mathcal{P}_\mathcal{R}$ with a log-normal width of $\sigma = 0.5$, set by the BBN and GW observations, e.g., EPTA (European Pulsar Timing Array) and aLIGO (Advanced LIGO, Inomata & Nakama 2019). Our PBB results constrain $\mathcal{P}_\mathcal{R} \lesssim 0.28$, which is the strongest $\mathcal{P}_\mathcal{R}$ limit for $k \in [10^8,\ 10^{22}]\,\mathrm{Mpc}^{-1}$ to date. Projected limits from S4 further tighten to $\mathcal{P}_\mathcal{R} \lesssim 0.11$. Future GW detectors such as Taiji (Hu & Wu 2017), TianQin (Luo et al. 2016), LISA (Amaro-Seoane et al. 2017), and the Square Kilometre Array (Carilli & Rawlings 2004; Janssen et al. 2015; Moore et al. 2015) can probe k between 10^5 and $10^{14}\,\mathrm{Mpc}^{-1}$ (Chen et al. 2021), potentially improving our constraints further.

As with the majority of PBH formation theories (Dolgov & Silk 1993; Yokoyama 1998b; Niemeyer & Jedamzik 1999; Green 2016; Carr et al. 2017; Bellomo et al. 2018; Pi et al. 2018), our PBHs follow an extended distribution and can be well described by the log-normal parameterization in Equation (7). Using the $\Omega_{\rm GW}(f_{\rm bh},\ \sigma_{\rm bh},\ M_{\rm bh})$ interpolation function described in the previous section, it can be shown numerically that $\Omega_{\rm GW}$ increases with $f_{\rm bh}$, and here we derive our $f_{\rm bh}$ upper bounds by iteratively solving Equation (14). In Figure 2 we show the $f_{\rm bh}$ limits for PBHs with distribution

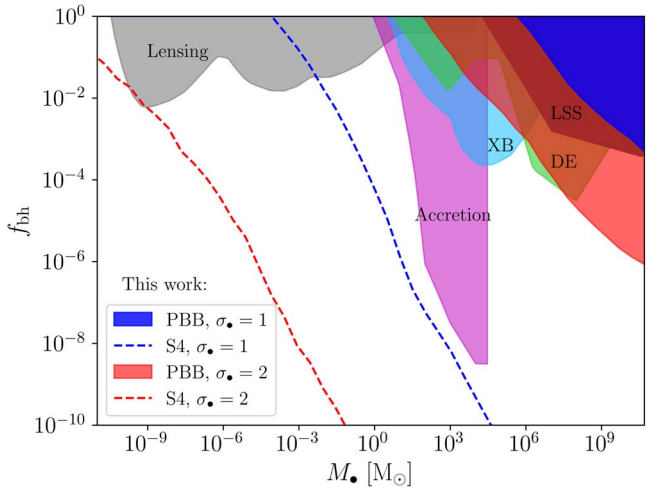

Figure 2. Bounds on $f_{\rm bh}$ as a function of PBH peak mass $M_\bullet$; the filled regions indicate the excluded parameter space. Our constraints are for PBHs produced by inflation-induced scalar perturbation, with the blue and red regions showing the current PBB exclusion bounds on PBHs with distribution widths of 1 and 2 respectively, whereas the blue ($\sigma_\bullet = 1$) and red ($\sigma_\bullet = 2$) dashed lines show the prospective limits from S4. All other limits in this figure are collected from Carr & Kuhnel (2020) and they apply to PBHs with a monochromatic distribution (i.e., $\sigma_\bullet = 0$) irrespective of their formation mechanism; from left to right, they are set by lensing (gray; Tisserand et al. 2007; Niikura et al. 2019), accretion (magenta; Serpico et al. 2020), X-ray binaries (XB, light blue; Inoue & Kusenko 2017), dynamical effects (DE, green; Lacey & Ostriker 1985; Carr & Sakellariadou 1999; Brandt 2016; Carr & Kuhnel 2020), and cosmological large-scale structure (LSS, brown; Carr & Silk 2018; Carr & Kuhnel 2020).

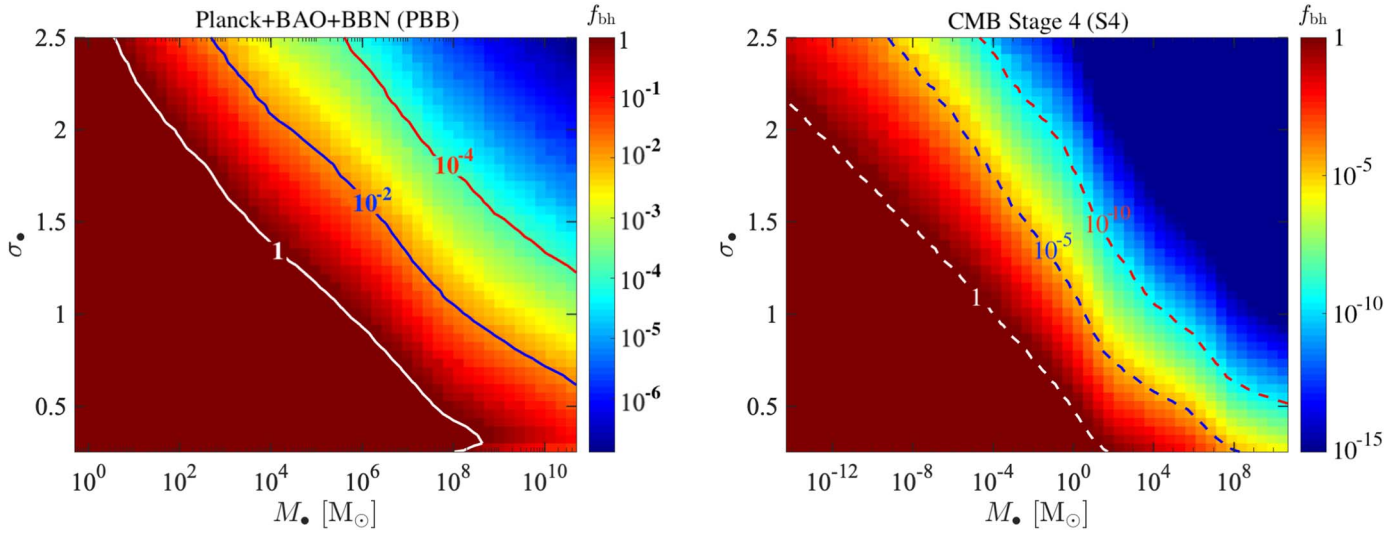

Figure 3. The 95% C.L. upper bounds on $f_{\rm bh}$ for different peak masses $M_\bullet$ and distribution widths $\sigma_\bullet$, applicable to PBHs formed from inflation-induced scalar perturbation. The left and right panels show the current PBB constraints and the prospective S4 limits respectively. The white contours indicate the parameter space where PBH can explain all dark matter ($f_{\rm bh} = 1$).

widths of $\sigma_\bullet = 1$ and $\sigma_\bullet = 2$, along with the existing bounds on monochromatic PBHs (assuming all PBHs having same mass) summarized in Carr & Kuhnel (2020) and Serpico et al. (2020). Note that in addition to the inflation-induced scalar perturbation, there are many other PBH formation scenarios (Carr et al. 2021b), e.g., collapse of cosmic strings (Hogan 1984; Hawking 1989; Polnarev & Zembowicz 1991; Hansen et al. 2000) and bubble collisions (Crawford & Schramm 1982; Hawking et al. 1982; La & Steinhardt 1989), thus caution should be taken while interpreting Figure 2. Our constraints apply to PBHs formed from enhanced scalar perturbation, whereas the rest of the limits constrain PBHs regardless of their formation mechanism.

For constraints from PBB with $\sigma_\bullet = 1$, the blue filled region in Figure 2 shows that it excludes supermassive PBHs with $M_\bullet \in [5 \times 10^5,\ 5 \times 10^{10}]\, M_\odot$ as the dominant DM component ($f_{\rm bh} < 1$), spanning over five orders of magnitude. The limit covers the range set by X-ray binaries (light blue; Inoue & Kusenko 2017) and LSS (brown; Carr & Kuhnel 2020). For $\sigma_\bullet = 2$, the PBB exclusion window expands to $[10^2,\ 5 \times 10^{10}]\, M_\odot$, which constitutes the widest PBH constraints to date. The red and blue dashed lines show the sensitivity of projected CMB-S4 experiment on PBH abundance, which can exclude PBHs of $[8 \times 10^{-5},\ 5 \times 10^{10}]\, M_\odot$ while setting the most stringent PBH constraints in a large mass range of $[7 \times 10^{-3},\ 5 \times 10^{10}]\, M_\odot$. Compared to other leading constraints in the supermassive PBH window around $[3 \times 10^4,\ 5 \times 10^{10}]\, M_\odot$, the limit from projected S4 can be stronger by more than 10 orders of magnitude. Figure 3 shows the complete constraints for a range of $\sigma_\bullet$ values. For fixed $f_{\rm bh}$, we find that $\Omega_{\rm GW}$ increases with both $\sigma_\bullet$ and $M_\bullet$, therefore our $f_{\rm bh}$ limit is tightened as we increase either $\sigma_\bullet$ or $M_\bullet$.

5. Summary

Scalar-perturbation-induced PBH formation events emit SIGWs that behave like a relativistic species, so that the measured $\Delta N_{\rm eff}$ can yield stringent limits on the scalar power spectra $\mathcal{P}_\mathcal{R}$ on small scales $10\ {\rm Mpc}^{-1} < k < 10^{22}\ {\rm Mpc}^{-1}$, much smaller than the direct measurement of CMB power spectra. Using a log-normal parameterization for $\mathcal{P}_\mathcal{R}$ arising from Horndeski gravity theory (Chen et al. 2021) (also a good approximation for a wide class of perturbation theories), we show that Planck CMB data combined with BBN and BAO data sets (PBB) give the currently most stringent $\mathcal{P}_\mathcal{R}$ constraints in $k \in [10^8,\ 10^{22}]\ {\rm Mpc}^{-1}$. For PBHs with a log-normal width of $\sigma_\bullet = 1$, PBB excludes supermassive PBHs with peak mass $M_\bullet \in [5 \times 10^5,\ 5 \times 10^{10}]\, M_\odot$ as the dominant DM component. Future CMB-S4 can probe the mass window $M_\bullet \in [8 \times 10^{-5},\ 5 \times 10^{10}]\, M_\odot$ and potentially improve $\mathcal{P}_\mathcal{R}$ limits of PBB by 60%.

J.C. and Y.G. acknowledge support from the National Natural Science Foundation of China (12275278), the China Scholarship Council (CSC, No.202104910395) and partially from the Ministry of Science and Technology of China (2020YFC2201601). Y.Z.M. is supported by the National Research Foundation of South Africa under grant Nos. 120385 and 120378, NITheCS program "New Insights into Astrophysics and Cosmology with Theoretical Models confronting Observational Data," and National Natural Science Foundation of China with project 12047503. J.C. thanks for the hospitality at the Cosmology Group of SNS during this project.

ORCID iDs

Yin-Zhe Ma https://orcid.org/0000-0001-8108-0986

References

Abazajian, K. N., Adshead, P., Aguirre, J., et al. 2016, arXiv:1610.02743
Abbott, B. P., Abbott, R., Abbott, T. D., et al. 2019, PhRvX, 9, 031040
Ade, P. A. R., Aghanim, N., Arnaud, M., et al. 2016, A&A, 594, A13
Aich, M., Ma, Y.-Z., Dai, W.-M., & Xia, J.-Q. 2020, PhRvD, 101, 063536
Aiola, S., Calabrese, E., Maurin, L., et al. 2020, JCAP, 12, 047
Ali-Haïmoud, Y., & Kamionkowski, M. 2017, PhRvD, 95, 043534
Amaro-Seoane, P., Audley, H., Babak, S., et al. 2017, arXiv:1702.00786
Ando, K., Inomata, K., & Kawasaki, M. 2018, PhRvD, 97, 103528
Ashoorioon, A., Rezazadeh, K., & Rostami, A. 2022, PhLB, 835, 137542
Ashoorioon, A., Rostami, A., & Firouzjaee, J. T. 2021a, JHEP, 07, 087
Ashoorioon, A., Rostami, A., & Firouzjaee, J. T. 2021b, PhRvD, 103, 123512
Auffinger, J. 2022, arXiv:2206.02672
Balkenhol, L., Dutcher, D., Spurio Mancini, A., et al. 2022, arXiv:2212.05642
Baumann, D., Green, D., Meyers, J., & Wallisch, B. 2016a, JCAP, 01, 007

Baumann, D., Green, D., & Wallisch, B. 2016b, PhRvL, 117, 171301
Bean, R., & Magueijo, J. 2002, PhRvD, 66, 063505
Bellomo, N., Bernal, J. L., Raccanelli, A., & Verde, L. 2018, JCAP, 01, 004
Belotsky, K. M., Dmitriev, A. D., Esipova, E. A., et al. 2014, MPLA, 29, 1440005
Belotsky, K. M., Dokuchaev, V. I., Eroshenko, Y. N., et al. 2019, EPJC, 79, 246
Brandt, T. D. 2016, ApJL, 824, L31
Bringmann, T., Scott, P., & Akrami, Y. 2012, PhRvD, 85, 125027
Byrnes, C. T., Cole, P. S., & Patil, S. P. 2019, JCAP, 06, 028
Cai, R.-G., Guo, Z.-K., Liu, J., Liu, L., & Yang, X.-Y. 2020, JCAP, 06, 013
Cang, J., Gao, Y., & Ma, Y.-Z. 2022, JCAP, 03, 012
Carbone, C., & Matarrese, S. 2005, PhRvD, 71, 043508
Carilli, C. L., & Rawlings, S. 2004, NewAR, 48, 979
Carr, B., Clesse, S., García-Bellido, J., & Kühnel, F. 2021a, PDU, 31, 100755
Carr, B., Kohri, K., Sendouda, Y., & Yokoyama, J. 2021b, RPPh, 84, 116902
Carr, B., & Kuhnel, F. 2020, ARNPS, 70, 355
Carr, B., & Kuhnel, F. 2022, ScPPL, 48, 1
Carr, B., Kuhnel, F., & Sandstad, M. 2016, PhRvD, 94, 083504
Carr, B., Raidal, M., Tenkanen, T., Vaskonen, V., & Veermäe, H. 2017, PhRvD, 96, 023514
Carr, B., & Silk, J. 2018, MNRAS, 478, 3756
Carr, B. J. 1975, ApJ, 201, 1
Carr, B. J., & Hawking, S. W. 1974, MNRAS, 168, 399
Carr, B. J., Kohri, K., Sendouda, Y., & Yokoyama, J. 2010, PhRvD, 81, 104019
Carr, B. J., & Sakellariadou, M. 1999, ApJ, 516, 195
Chacko, Z., Cui, Y., Hong, S., & Okui, T. 2015, PhRvD, 92, 055033
Chen, P., Koh, S., & Tumurtushaa, G. 2021, arXiv:2107.08638
Chen, Z.-C., Yuan, C., & Huang, Q.-G. 2020, PhRvL, 124, 251101
Clark, S., Dutta, B., Gao, Y., Ma, Y.-Z., & Strigari, L. E. 2018, PhRvD, 98, 043006
Clark, S., Dutta, B., Gao, Y., Strigari, L. E., & Watson, S. 2017, PhRvD, 95, 083006
Crawford, M., & Schramm, D. N. 1982, Natur, 298, 538
de Salas, P. F., & Pastor, S. 2016, JCAP, 07, 051
Di Valentino, E., Brinckmann, T., Gerbino, M. , et al. 2018, JCAP, 04, 017
Dolgov, A., & Silk, J. 1993, PhRvD, 47, 4244
Domènech, G. 2021, Univ, 7, 398
Domènech, G., Lin, C., & Sasaki, M. 2021a, JCAP, 04, 062
Domènech, G., Takhistov, V., & Sasaki, M. 2021b, PhLB, 823, 136722
Efstathiou, G. 2020, arXiv:2007.10716
Efstathiou, G. 2021, MNRAS, 505, 3866
Follin, B., Knox, L., Millea, M., & Pan, Z. 2015, PhRvL, 115, 091301
Freedman, W. L., Madore, B. F., Hoyt, T., et al. 2020, ApJ, 891, 57
Garcia-Bellido, J., & Ruiz Morales, E. 2017, PDU, 18, 47
Green, A. M. 2016, PhRvD, 94, 063530
Green, A. M., & Kavanagh, B. J. 2021, JPhG, 48, 043001
Green, D., Amin, M. A., Meyers, J., et al. 2019, BAAS, 51, 159
Hanany, S., Alvarez, M., Artis, E., et al. 2019, BAAS, 51, 194
Hansen, R. N., Christensen, M., & Larsen, A. L. 2000, IJMPA, 15, 4433
Harada, T., Yoo, C.-M., & Kohri, K. 2013, PhRvD, 88, 084051
Hawking, S. 1971, MNRAS, 152, 75
Hawking, S. W. 1989, PhLB, 231, 237
Hawking, S. W., Moss, I. G., & Stewart, J. M. 1982, PhRvD, 26, 2681
Hogan, C. J. 1984, PhLB, 143, 87
Hou, Z., Keisler, R., Knox, L., Millea, M., & Reichardt, C. 2013, PhRvD, 87, 083008
Hu, W.-R., & Wu, Y.-L. 2017, Natl. Sci., 4, 685
Hunt, P., & Sarkar, S. 2015, JCAP, 12, 052
Hütsi, G., Raidal, M., Vaskonen, V., & Veermäe, H. 2021, JCAP, 03, 068
Inomata, K., Kawasaki, M., Mukaida, K., Tada, Y., & Yanagida, T. T. 2017, PhRvD, 96, 043504
Inomata, K., & Nakama, T. 2019, PhRvD, 99, 043511
Inoue, Y., & Kusenko, A. 2017, JCAP, 10, 034
Janssen, G. H., Hobbs, G., McLaughlin, M., et al. 2015, in Proc. of Advancing Astrophysics with the Square Kilometre Array (AASKA14) (Trieste: SISSA), 37
Jedamzik, K. 2021, PhRvL, 126, 051302
Josan, A. S., Green, A. M., & Malik, K. A. 2009, PhRvD, 79, 103520
Kannike, K., Marzola, L., Raidal, M., & Veermäe, H. 2017, JCAP, 09, 020
Karam, A., Koivunen, N., Tomberg, E., Vaskonen, V., & Veermäe, H. 2023, JCAP, 2023, 013
Kawasaki, M., Sugiyama, N., & Yanagida, T. 1998, PhRvD, 57, 6050
Khlopov, M. Y. 2010, RAA, 10, 495
Kimura, R., Suyama, T., Yamaguchi, M., & Zhang, Y.-L. 2021, JCAP, 04, 031
Kohri, K., Lin, C.-M., & Matsuda, T. 2013, PhRvD, 87, 103527
Kohri, K., & Terada, T. 2018, PhRvD, 97, 123532
Kolb, E. W., & Turner, M. S. 1990, The Early Universe (Boca Raton, FL: CRC Press)
La, D., & Steinhardt, P. J. 1989, PhLB, 220, 375
Lacey, C. G., & Ostriker, J. P. 1985, ApJ, 299, 633
Laha, R. 2019, PhRvL, 123, 251101
Laha, R., Muñoz, J. B., & Slatyer, T. R. 2020, PhRvD, 101, 123514
Luo, J., Chen, L.-S., Duan, H.-Z., et al. 2016, CQGra, 33, 035010
Mangano, G., Miele, G., Pastor, S., et al. 2005, NuPhB, 729, 221
Mangano, G., Miele, G., Pastor, S., & Peloso, M. 2002, PhLB, 534, 8
Meerburg, P. D., Hložek, R., Hadzhiyska, B., & Meyers, J. 2015, PhRvD, 91, 103505
Mittal, S., Ray, A., Kulkarni, G., & Dasgupta, B. 2022, JCAP, 03, 030
Moore, C. J., Cole, R. H., & Berry, C. P. L. 2015, CQGra, 32, 015014
Musco, I., & Miller, J. C. 2013, CQGra, 30, 145009
Nakama, T., Silk, J., & Kamionkowski, M. 2017, PhRvD, 95, 043511
Nakamura, K. 2007, PThPh, 117, 17
Niemeyer, J. C., & Jedamzik, K. 1999, PhRvD, 59, 124013
Niikura, H., Takada, M., Yasuda, N., et al. 2019, NatAs, 3, 524
Özsoy, O., Parameswaran, S., Tasinato, G., & Zavala, I. 2018, JCAP, 07, 005
Pi, S., & Sasaki, M. 2020, JCAP, 09, 037
Pi, S., Zhang, Y.-l., Huang, Q.-G., & Sasaki, M. 2018, JCAP, 05, 042
Planck Collaboration, Aghanim, N., Akrami, Y., et al. 2020, A&A, 641, A6
Polnarev, A., & Zembowicz, R. 1991, PhRvD, 43, 1106
Press, W. H., & Schechter, P. 1974, ApJ, 187, 425
Ray, A., Laha, R., Muñoz, J. B., & Caputo, R. 2021, PhRvD, 104, 023516
Riess, A. G., Yuan, W., Macri, L. M., et al. 2022, ApJL, 934, L7
Riess, A. G., Macri, L.M., Hoffmann, S.L., et al. 2016, ApJ, 826, 56
Riess, A. G., Casertano, S., Yuan, W., et al. 2018, ApJ, 855, 136
Schöneberg, N., Verde, L., Gil-Marín, H., & Brieden, S. 2022, JCAP, 2022, 039
Serpico, P. 2019, PoS, 347, 094
Serpico, P. D., Poulin, V., Inman, D., & Kohri, K. 2020, PhRvR, 2, 023204
Takahashi, F., & Yamada, M. 2019, JCAP, 07, 001
Tashiro, H., & Sugiyama, N. 2013, MNRAS, 435, 3001
Tisserand, P., Guillou, L. L., Afonso, C., et al. 2007, A&A, 469, 387
Vaskonen, V., & Veermäe, H. 2021, PhRvL, 126, 051303
Verde, L., Treu, T., & Riess, A. G. 2019, NatAs, 3, 891
Wallisch, B. 2018, PhD thesis, Cambridge Univ. doi:10.17863/CAM.30368
Wang, S., Wang, Y.-F., Huang, Q.-G., & Li, T. G. F. 2018, PhRvL, 120, 191102
Wang, X., Zhang, Y.-l., Kimura, R., & Yamaguchi, M. 2023, SCPMA, 66, 260462
Yang, Y. 2021, PhRvD, 104, 063528
Yokoyama, J. 1998a, PhRvD, 58, 083510
Yokoyama, J. 1998b, PhRvD, 58, 107502
Young, S., Byrnes, C. T., & Sasaki, M. 2014, JCAP, 07, 045
Yuan, C., & Huang, Q.-G. 2021, iSci, 24, 102860
Zhou, H., Lian, Y., Li, Z., Cao, S., & Huang, Z. 2022, MNRAS, 513, 3627